Report

Co$_3$Mo$_3$N—An efficient multifunctional electrocatalyst

Yao Yuan,[1,2,7] Samira Adimi,[1,7] Tiju Thomas,[3] Jiacheng Wang,[4] Haichuan Guo,[1] Jian Chen,[2] J. Paul Attfield,[5,*] Francis J. DiSalvo,[6,*] and Minghui Yang[1,*]

*Correspondence: j.p.attfield@ed.ac.uk (J.P.A.); fjd3@cornell.edu (F.J.D.); myang@nimte.ac.cn (M.Y.)

Graphical abstract

Public summary

- Porous Co$_3$Mo$_3$N can act as a multifunctional electrocatalyst for OER, ORR, and HER

- Co$_3$Mo$_3$N performs better than precious metal catalysts

- Cobalt oxide-rich activation surface layer is shown to aid OER activity

- Better ORR and HER performance of Co$_3$Mo$_3$N is due to Co and Mo d-states
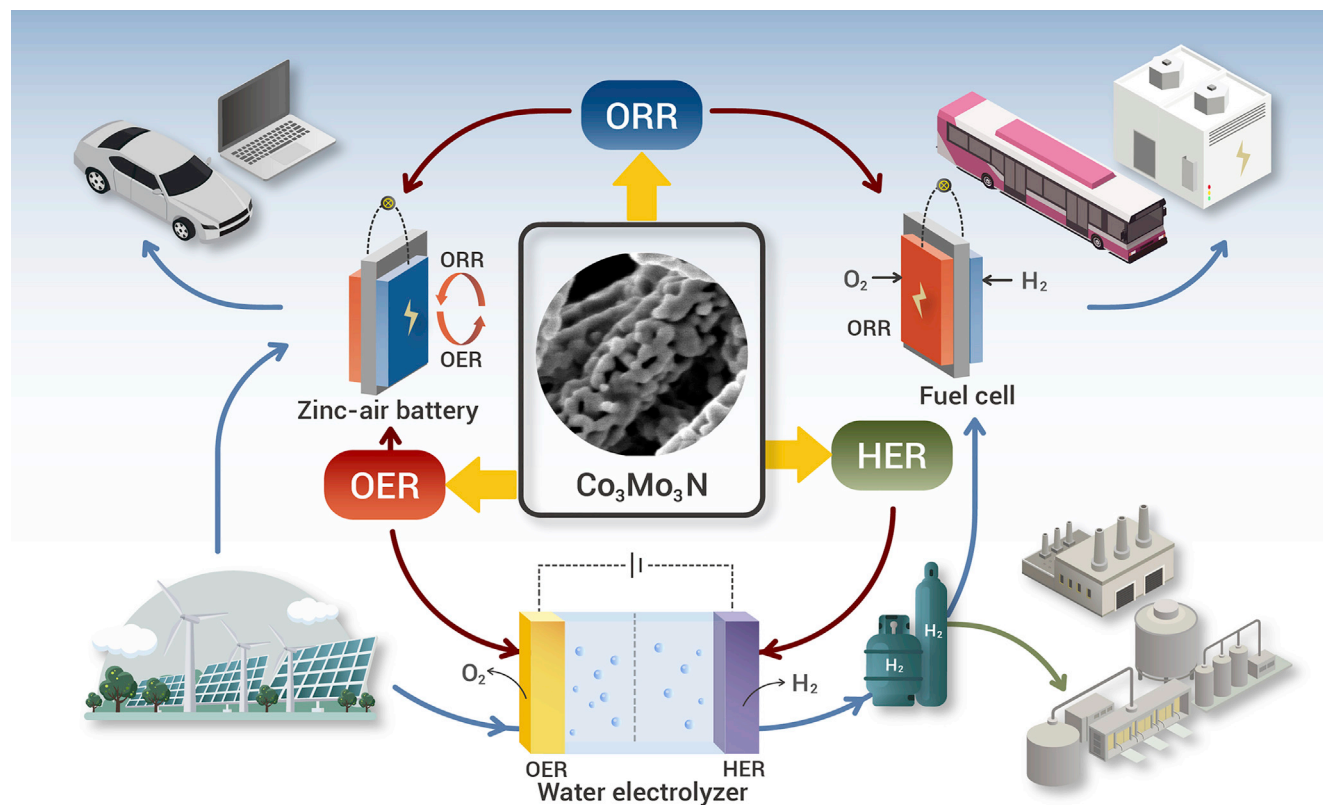
Co₃Mo₃N—An efficient multifunctional electrocatalyst

Yao Yuan,[1,2,7] Samira Adimi,[1,7] Tiju Thomas,[3] Jiacheng Wang,[4] Haichuan Guo,[1] Jian Chen,[2] J. Paul Attfield,[5,*] Francis J. DiSalvo,[6,*] and Minghui Yang[1,*]

[1]Ningbo Institute of Materials Technology and Engineering, Chinese Academy of Sciences, Ningbo, 315201, China

[2]Dalian Institute of Chemical Physics, Chinese Academy of Sciences, Dalian, 116023, China

[3]Department of Metallurgical and Materials Engineering, Indian Institute of Technology Madras Adyar, Chennai 600036, Tamil Nadu, India

[4]State Key Laboratory of High Performance Ceramics and Superfine Microstructure, Shanghai Institute of Ceramics, Chinese Academy of Sciences, Shanghai, 200050, China

[5]Centre for Science at Extreme Conditions and School of Chemistry, University of Edinburgh, Edinburgh, EH9 3JZ, UK

[6]Department of Chemistry and Chemical Biology, Cornell University, New York, 14853, USA

[7]These authors contributed equally

*Correspondence: j.p.attfield@ed.ac.uk (J.P.A.); fjd3@cornell.edu (F.J.D.); myang@nimte.ac.cn (M.Y.)

Citation: Yuan Y., Adimi S., Thomas T., et al., (2021). Co₃Mo₃N—An efficient multifunctional electrocatalyst. The Innovation 2(2), 100096.

Efficient catalysts are required for both oxidative and reductive reactions of hydrogen and oxygen in sustainable energy conversion devices. However, current precious metal-based electrocatalysts do not perform well across the full range of reactions and reported multifunctional catalysts are all complex hybrids. Here, we show that single-phase porous Co_3Mo_3N prepared via a facile method is an efficient and reliable electrocatalyst for three essential energy conversion reactions; oxygen evolution reaction (OER), oxygen reduction reaction (ORR), and hydrogen evolution reaction (HER) in alkaline solutions. Co_3Mo_3N presents outstanding OER, ORR, and HER activity with high durability, comparable with the commercial catalysts RuO_2 for OER and Pt/C for ORR and HER. In practical demonstrations, Co_3Mo_3N gives high specific capacity (850 mA h g_{Zn}^{-1} at 10 mA cm^{-2}) as the cathode in a zinc-air battery, and a low potential (1.63 V at 10 mA cm^{-2}) used in a water-splitting electrolyzer. Availability of Co and Mo d-states appear to result in high ORR and HER performance, while the OER properties result from a cobalt oxide-rich activation surface layer. Our findings will inspire further development of bimetallic nitrides as cost-effective and versatile multifunctional catalysts that will enable scalable usage of electrochemical energy devices.

KEYWORDS: ternary nitrides; multifunctional electrocatalysts; rechargeable Zn-air batteries; water splitting

INTRODUCTION

Electrode reactions are involved in new energy technologies for efficient energy conversion, storage, and management, such as fuel cells,[1,2] metal-air batteries,[3,4] and water-splitting electrolyzers.[5] However, sluggish kinetics with high overpotential tends to limit these technologies. Typically, these challenges escalate further when multi-electron transfer processes are associated with the electrocatalytic reactions.[6,7] Noble metal-based catalysts (such as Pt, Ru, and Ir) are currently considered as the state-of-the-art catalysts. Pt is used in oxygen reduction reaction (ORR) and hydrogen evolution reaction (HER). Ru/Ir-based materials on the other hand are useful for oxygen evolution reaction (OER).[8–11] However, high cost, scarcity, and unsatisfactory durability of these noble metal-based materials limit their viability and scalable use for renewable energy technologies.[12–14]

Cheap and multifunctional catalysts that can accelerate all three ORR, HER, and OER would be desirable. Examples include rechargeable metal-air batteries that combine ORR and OER, and water electrolyzers that combine HER and OER. This also has significant implications for scalability since single-phase multifunctional catalysts can reduce materials flow concerns and simplify the manufacture of the system. Thus far, the few reports on multifunctional catalysts involve complex hybrids (e.g., graphitic-shell

$Fe_xCo_yNi_z$ alloys,[15] GO-Cu-MOF,[16] Mo-N/C@MoS₂,[17] Co₂P/CoN/C,[18] and defect graphene).[19] Interstitial metal nitrides are an interesting class of materials with their unique mechanical, magnetic, electrical, and catalyzed active properties.[20] In a number of cases, the catalytic performance of nitrides is analogous with that of noble metals, due to their very similar Fermi energy and electronic structure to that of group VIII noble metals.[21] However, until now no single-phase nitride has demonstrated multifunctional electrocatalysis. As Co_3Mo_3N, has already found catalytic use in lithium-O₂ batteries,[22–24] CO₂ reforming,[25] hydrazine synthesis,[26] hydrodesulfurization,[27] ammonia synthesis, and decomposition,[28–30] we have investigated its use as a multifunctional electrocatalyst.[31] Here, a porous Co_3Mo_3N catalyst is synthesized via a simple and generally applicable strategy and demonstrates high activity for ORR, HER, and OER.

RESULTS AND DISCUSSION

Co_3Mo_3N is prepared in a straightforward manner through ammonolysis of $CoMoO_4$ at 800°C (Figures S1 and S2A). As shown in the Rietveld refinement results, the as-prepared Co_3Mo_3N forms an intermediate nitride with an η-carbide-like cubic structure (in space group: *Fd-3m*, a = 11.0132(1) Å) (Figure 1A; Table S1). In fact there are two interpenetrating networks of corner-shared NMo₆ octahedra and Co[Mo₆Co₆]/Co[Mo₆Co₄N₂] pseudo-icosahedra in the Co_3Mo_3N structure (Figure S3).[32] Co_3Mo_3N comprises one-dimensional porous rods with diameters in the range 100–300 nm (Figures 1, S2B, and S4). Also, the results of high-resolution transmission electron microscopy (HR-TEM) and electron energy loss spectroscopy (EELS) mapping suggest that there is no distinct phase or shell on the surface (Figures 1D and 1E). The polycrystalline nature of Co_3Mo_3N is proven using selected area electron diffraction pattern with diffracted spots as shown in Figure S5, and the percentages of elements in Co_3Mo_3N are determined by an inductively coupled plasma optical emission spectrometer and an elemental analyzer (Tables S2 and S3).

The electrocatalytic performance for three energy conversion processes (ORR, HER, and OER) of Co_3Mo_3N was investigated under standard conditions with the alkaline electrolyte (Figure 2). Figure 2A shows the ORR polarization curves of Co_3Mo_3N, measured in 0.1 M KOH. Co₄N, Mo₃N₂ (see the supplemental information and Figure S6 for more details) and the commercial 20 wt.% Pt/C (the industry standard ORR catalyst) are tested using same conditions for comparison. The half-wave potential ($E_{1/2}$) of Co_3Mo_3N (0.75 V) is lower than that of commercial Pt (0.80 V), but more positive than those of the binary nitrides Co₄N (0.65 V) and Mo₃N₂ (0.66 V). In the range of 0.2–0.8 V, almost ideal four-electron reduction takes place (calculated number of transferred electrons $n \approx 3.8$) and the peroxide yield observed is low (6%–10%) (Figure S7). Koutecky-Levich analysis confirms this mechanism, as seen in the deduced $n = 3.9$ (Figure S8). The reaction dynamics can be
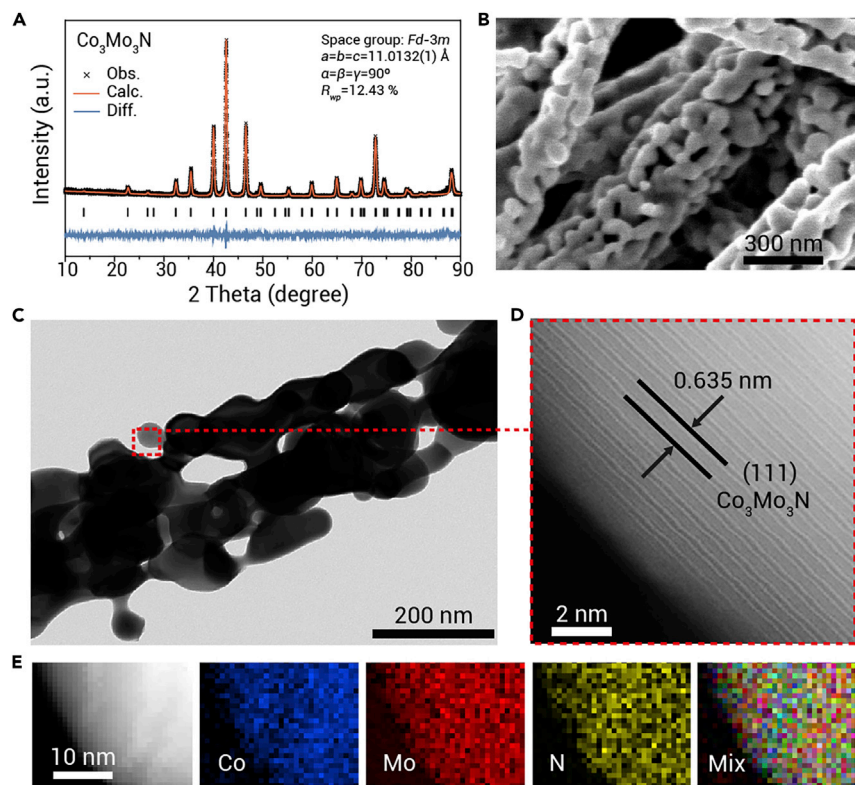
Figure 1. Characterization of as-prepared porous Co₃Mo₃N rods (A) Rietveld fitted XRD pattern of Co₃Mo₃N.
(B−D) (B) SEM and (C) TEM images of porous Co₃Mo₃N rods and (D) the corresponding HR-TEM image. Lattice spacing is 0.635 nm corresponding to the (111) plane of cubic Co₃Mo₃N with no distinct surface phases.
(E) HAADF-STEM and EELS images of Co, Mo, and N elements for the Co₃Mo₃N sample. The results show a homogeneous elemental distribution without any surface phase.

studied using the Tafel slope. As seen in Figure 2B, Co₃Mo₃N displays a smaller Tafel slope (57 mV dec⁻¹) when compared with than 20 wt.% Pt/C (81 mV dec⁻¹), demonstrating better ORR catalytic kinetics.

The HER activity of the same materials is also evaluated in the alkaline electrolyte (1.0 M KOH), and all polarization curves are corrected for internal Ohmic losses (*iR*-corrections). From the linear sweep voltammograms (LSVs) (Figure 2C), it is seen that an overpotential to achieve a catalytic current density of 10 mA cm⁻² (η_{10}) is −0.10 V for Co₃Mo₃N compared with −0.01 V for Pt/C under identical conditions. However, and importantly, the current densities of Co₃Mo₃N and Pt/C reach the same value at −0.30 V, demonstrating excellent properties of the Co₃Mo₃N catalyst under large currents. Co₃Mo₃N also shows much higher activity than Co₄N (η_{10} = −0.16 V) and Mo₃N₂ (η_{10} = −0.21 V). The Tafel slope of Co₃Mo₃N (49 mV dec⁻¹) is lower than those of Co₄N (111 mV dec⁻¹) and Mo₃N₂ (81 mV dec⁻¹) as shown in Figure 2D. This is evidence of improved kinetics and better HER activity through the use of Co₃Mo₃N.

The OER activity of Co₃Mo₃N was also evaluated using linear sweep voltammetry. The results for Co₄N, Mo₃N₂, CoMoO₄, and RuO₂ (one of the best known active OER catalysts) are used as a benchmark for comparison (Figures 2E and S9). The LSV curves with *iR*-correction indicate that the OER activity of Co₃Mo₃N is better than those of Co₄N, Mo₃N₂, and CoMoO₄. In fact, the performance even exceeds that of RuO₂ significantly. To generate a catalytic current density of 10 mA cm⁻², η_{10} values required for Co₃Mo₃N, Co₄N, Mo₃N₂, CoMoO₄, and RuO₂ are 0.29, 0.33, 0.43, 0.41, and 0.35 V, respectively (Figure 2E inset). And their respective Tafel slopes are 60, 75, 93, 102, and 86 mV dec⁻¹ (Figures 2F and S9). Hence, Co₃Mo₃N outperforms RuO₂ as well as the binary nitrides (Co₄N and Mo₃N₂) and oxide (CoMoO₄) for OER. Above all, Co₃Mo₃N exhibits small overpotentials and high currents for all three electrocatalytic reactions and is more stable compared with the commercial precious metal-based catalysts (Figure S10).

The good ORR and HER performances can be explained by the electronic structures. Binary transition metal nitrides (such as iron, cobalt, and nickel nitrides) have previously been studied as non-precious-metal catalysts.[33] The electrocatalytic activity of cobalt hydroxide toward HER and OER was investigated theoretically, showing that the hybridization of 2p states of O atom and 3d states of Co atoms plays crucial roles in charge transfer and also increases the metallic property of the Co hydroxide layer.[34] Moreover, density functional theory (DFT) calculations were applied to explore the active sites of Co₃Mo₃N toward hydrogen adsorption on top of the (111) surfaces.[35,36] The results show that molecular hydrogen would be adsorbed mostly on the MoN₃ framework, binding through the Mo atoms, and dissociative hydrogen adsorptions would occur on exposed cobalt atoms of Co₈ clusters or occur on Mo₃ clusters that are close to N vacancies. DFT calculations also have indicated that heavier transition metals, such as molybdenum or tungsten, modify the electronic structure of nitrides favorably.[37] This leads to near-optimal adsorption of intermediates in electrochemical reactions and hence improved catalytic activity.[38] Co₃Mo₃N, with an η-carbide structure, is a metallic nitride with enhanced d-states density near the Fermi level, as shown in Figure S11. This is in contrast to Co₄N, whose electronic states are more p-like around the Fermi level (contributed from nitrogen) (Figure S11). After adding Mo atoms to the Co₄N structure, there is a charge transfer from Mo to Co species (Figures S11A and S11C). In comparison with Mo₃N₂, a lower Mo valence in Co₃Mo₃N is due to the lower occupation of Mo in the d-band. This in fact is expected to give an electron-donating ability to the Co₃Mo₃N crystal, and therefore enhancing kinetics of ORR and HER. Hence its unique electronic structure makes Co₃Mo₃N a promising candidate for ORR and HER (as also evidenced by experiment). In addition, it is noted that the d-band center[39] is a good gauge in designing active oxygen and hydrogen reaction catalysts. This measure involves the determination of the first moment of the projected d-band density of states relative to the Fermi level. By considering this parameter, Co₃Mo₃N (with a d-band center of −1.61 eV) should be a better OER catalyst than Ru (whose d-band center is around −1.42 eV).[40] This too is consistent with our experimental results.

It is surprising to have good OER activity as well as desirable ORR and HER performances in one material. To help explain the high activities of Co₃Mo₃N, the catalysts are investigated using XRD and X-ray photoelectron spectroscopy (XPS) analysis before and after cycling. The XRD pattern of Co₃Mo₃N after OER process shows the additional peaks compared with the initial sample, which proves that the surface oxidization occurs during the OER process without morphology changes (Figures S12 and S13). Also, there is no obvious
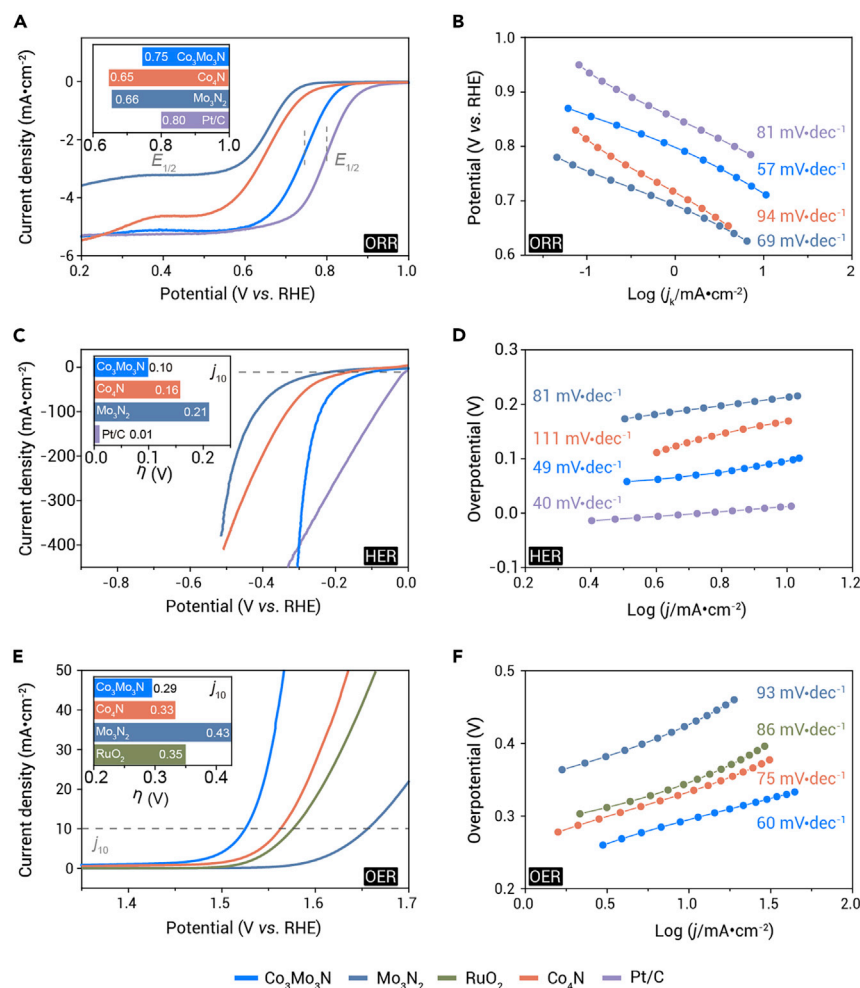
Figure 2. ORR, HER, and OER catalysis properties of Co$_3$Mo$_3$N, Co$_4$N, Mo$_3$N$_2$, 20% Pt/C, and RuO$_2$ in alkaline solution (A) ORR polarization curves in O$_2$-saturated 0.1 M KOH solution (10 mV s^{-1}) and comparison of half-wave potentials for ORR (inset).
(B) Corresponding ORR Tafel plots.
(C) Polarization curves for HER (10 mV s^{-1}) using carbon paper electrode in 1.0 M KOH solution and comparison of overpotentials required to achieve 10 mA cm^{-2} for HER (inset).
(D) Corresponding HER Tafel plots.
(E) Polarization curves for OER in 1.0 M KOH solution (10 mV s^{-1}) and comparison of overpotentials required to achieve 10 mA cm^{-2} (inset).
(F) Corresponding OER Tafel plots.

change for both Co 2p and Mo 3d after ORR and HER processes (Figures S14 and S15), but change is observed after OER. Hence, we perform analysis using TEM. Deconvolution of Co 2p spectra can be ascribed to Co-N species and Co^{2+} (Co-O) with a pair of satellite peaks (Figure 3).[18,41] Co-N peaks disappear after OER testing, which indicates oxidation of Co atoms occurs on the Co$_3$Mo$_3$N surface. Mo 3d region XPS spectra can be resolved into three types of peaks associated to Mo-N, Mo^{4+}, and Mo^{6+}, respectively.[42–44] All types of Mo 3d (including Mo-N) peaks remain, although with weaker intensity (Figure S15), suggesting that Mo atoms coordinated by N are present in the subsurface. Detailed analysis of the surface layer of Co$_3$Mo$_3$N after OER cycles is further confirmed using TEM. The as-prepared sample shows no additional surface layer but, after the OER, an amorphous oxide/hydroxide layer (~3–6 nm) appears on the surface. The HR-TEM image, high-angle annular dark field-scanning TEM (HAADF-STEM) image and the corresponding EELS elemental mappings show that the topmost part of the surface oxide layer is enriched in Co (Figures 3C–3E). According to this, an amorphous cobalt oxide-rich activation surface layer is generated on Co$_3$Mo$_3$N during OER process, which offers the active sites for OER.[33,45–47] Specifically, the Mo atoms shift toward the inner bulk forming short bonding with N atoms to compensate the influence of dangling bonds in surface. The surface Co atoms get more freedom to be oxidized, which are also expected to offer flexible valence during OER runs, and hence is likely the key source of catalytic activity (Figure 3A). The electronic states of Co in the oxide-rich surface can be tuned by the local oxide/nitride composition which shifts the position and width of the d-electron band. The deprotonation of OH for OER over the Ni/Co-based materials is normally considered the potential determining step. The cobalt oxide-rich surface can offer favorable ener-

getics for the deprotonation of OH.[47] Meanwhile, the surface Mo atoms can transfer charges and facilitate the reaction continuity as an electron pump.[47] These, in fact, are expected to offer the appropriate energetics and electronic structures for advanced catalytic efficiency.

Inspired by the remarkable half-cell performance of Co$_3$Mo$_3$N as a multifunctional catalyst for ORR, HER, and OER simultaneously, a circuit consisting of a rechargeable zinc-air battery and a water electrolyzer has been built (Video S1). This was done to demonstrate the utility of the multifunctional Co$_3$Mo$_3$N electrocatalyst in practical applications. The zinc-air battery with a Co$_3$Mo$_3$N cathode was fabricated as shown in Figure S16A. As a rechargeable battery, the charging process of the zinc-air battery is supported by OER on the cathode side, while ORR happens in the discharging process. Thus, efficient catalysts for both ORR and OER simultaneously are vital in this case. Conventionally, the fabrication of the electrode uses a mixture of ORR and OER catalysts. Here, we offer a simpler manufacturing approach, as the as-synthesized single-phase Co$_3$Mo$_3$N is the only catalyst for anode and cathode fabrication.

For comparison, a control zinc-air battery was fabricated with a precious metal-based air-cathode using the commercial Pt/C and RuO$_2$ composite. As illustrated in Figure 4A, the Co$_3$Mo$_3$N-driven zinc-air battery shows a smaller voltage gap in the charge and discharge polarization curves compared with the commercial Pt/C and RuO$_2$ composite catalyst demonstrating excellent cyclability. Galvanostatic discharge curves of a Co$_3$Mo$_3$N-driven zinc-air battery at various current densities from 2 to 50 mA cm^{-2} are illustrated to explore the discharge rate performance. As shown in Figure S16B, the discharge potential recovers when the current density goes back to 2 mA cm^{-2}, suggesting good rate capability. Specific capacity can
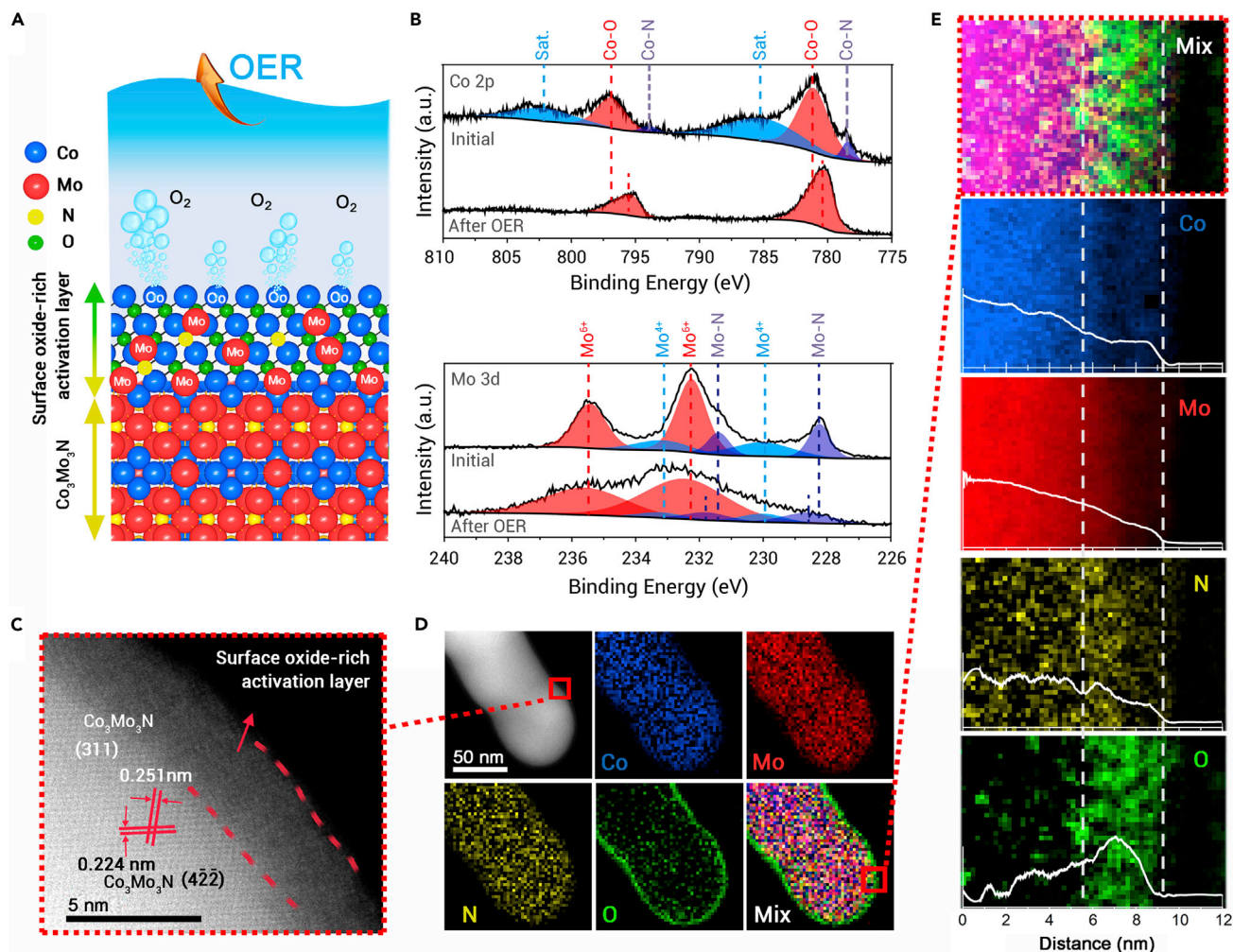
Figure 3. Characterization of Co₃Mo₃N catalyst after the OER process (A) Schematic illustration of the cobalt oxide-rich activation surface layer generated during the OER process. (B) Co 2p region and Mo 3d region XPS spectra of Co_3Mo_3N before and after OER cycles. (C) HR-TEM image of Co_3Mo_3N after OER cycles. (D and E) Typical HAADF-STEM, EELS element mapping of Co_3Mo_3N after the OER cycles with the corresponding EELS line-scan profiles of the cobalt oxide-rich activation surface layer.

be obtained according to the consumption of zinc. At 10 mA cm⁻², the Co_3Mo_3N-driven zinc-air battery gives a specific capacity of 850 mA h g_{Zn}^{-1}, which outperforms the Pt/C and RuO_2 battery (755 mA h g_{Zn}^{-1}) (Figure S16C). For stability, the charge-discharge voltage gap of the commercial Pt/C and RuO_2 composite system increases greatly after 100 h; on the other hand, the voltage gap for Co_3Mo_3N remains stable at a current density of 2 mA cm⁻² (Figure 4B). Compared with the voltage gap (0.84 V) after 50 h, the discharge-charge potential gap of Co_3Mo_3N-based battery only increases by 0.05 and 0.12 V after 150 and 260 h, respectively. To examine the air-cathode's cycling stability at a higher current density, we tested the two batteries at a current density of 10 mA cm⁻² (Figure S16D). Co_3Mo_3N-based battery still shows a slightly increased potential gap demonstrating the ultralong cycling ability, while a commercial Pt/C and RuO_2-based battery displays a significant variation in both charge and discharge voltages. This result shows the stability of Co_3Mo_3N when employed in operation as a cathode of zinc-air battery.

The water-splitting performance of Co_3Mo_3N catalyst has been further discussed in a two-electrode setup fabricated with both a Co_3Mo_3N-based anode and cathode. As illustrated in the LSV curves (Figure 4C), a current density of 10 mA cm⁻² can be obtained at around 1.63 V for Co_3Mo_3N-based electrodes. Although a slightly lower potential (1.61 V) is required to achieve 10 mA cm⁻² in the commercial RuO_2 and Pt/C-based electrolyzer, the observed current density reaches the same value as the Co_3Mo_3N at 1.68

V. For stability, Co_3Mo_3N when operated at an applied potential of 1.63 V to reach 10 mA cm⁻², shows only a slight degradation over a 24 h testing period (Figure 4D). The excellent results for practical devices further demonstrate the high promise of the reported single-phase ternary nitride electrocatalyst. It offers a way toward cost-effective, stable, and high-performance electrocatalytic materials.

Conclusions

In summary, single-phase porous Co_3Mo_3N is found to be an excellent multifunctional electrocatalyst for ORR, HER, and OER. Co_3Mo_3N shows better ORR and HER performance than the corresponding binary nitride phases and Pt/C due to the presence of both 3d and 4d contributions to the band structure. A cobalt oxide-rich surface layer offers flexible valence, modifying the band energy for good OER activity, which shows more advanced performance than most of the reported catalysts and the RuO_2 benchmark. We demonstrate the multifunctional nature of Co_3Mo_3N in a practical combination of a rechargeable zinc-air battery and water electrolyzer where stability and performance indicators surpass the state-of-the-art precious metal-based catalysts. It will reveal a new direction for future design of multifunctional catalysts using bimetallic nitrides as cost-effective, stable, and versatile materials that will offer prospects for scalable usage of electrochemical energy devices.
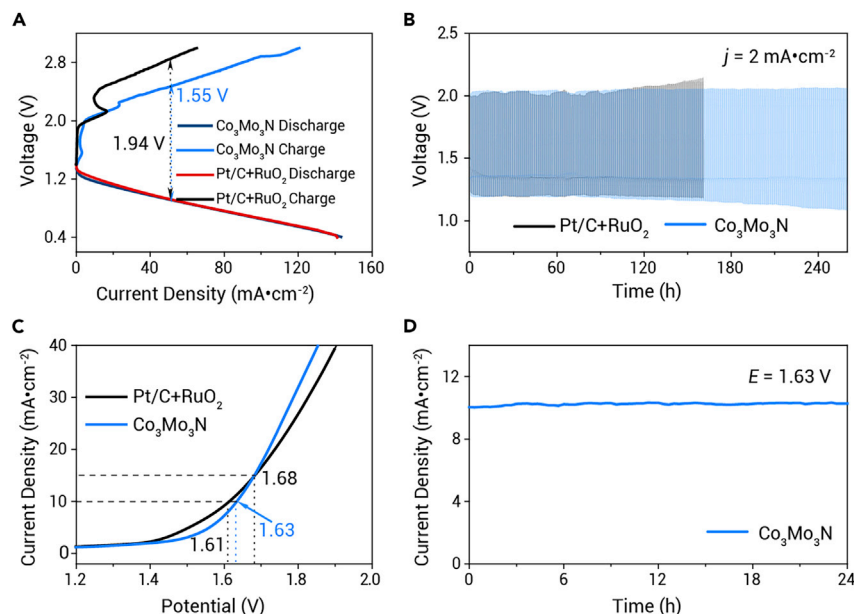
Figure 4. Zinc-air batteries and water-splitting electrolyzers using Co_3Mo_3N or combined Pt/C and RuO_2 catalysts
(A) Charge and discharge polarization curves of the zinc-air batteries.
(B) Long-term cycling curves at a constant current density of 2 mA cm^{-2} with a pulse cycling interval of 30 min per cycle.
(C) Polarization curves of an alkaline electrolyzer for the overall water-splitting reaction.
(D) Potentiostatic electrolysis for water-splitting reaction at a constant voltage of 1.63 V.

REFERENCES

1. Yang, M., Guarecuco, R., and DiSalvo, F.J. (2013). Mesoporous chromium nitride as high performance catalyst support for methanol electrooxidation. Chem. Mater. **25**, 1783–1787.
2. Strasser, P., Koh, S., Anniyev, T., et al. (2010). Lattice-strain control of the activity in dealloyed core-shell fuel cell catalysts. Nat. Chem. **2**, 454–460.
3. Xiao, J., Mei, D., Li, X., et al. (2011). Hierarchically porous graphene as a lithium-air battery electrode. Nano Lett. **11**, 5071–5078.
4. He, P., Wang, Y., and Zhou, H. (2011). Titanium nitride catalyst cathode in a Li−air fuel cell with an acidic aqueous solution. Chem. Commun. **47**, 10701–10703.
5. Park, S., Shao, Y., Liu, J., et al. (2012). Oxygen electrocatalysts for water electrolyzers and reversible fuel cells: status and perspective. Energ. Environ. Sci. **5**, 9331–9344.
6. Zou, X., and Zhang, Y. (2015). Noble metal-free hydrogen evolution catalysts for water splitting. Chem. Soc. Rev. **44**, 5148–5180.
7. Zhu, Y.P., Guo, C., Zheng, Y., et al. (2017). Surface and interface engineering of noble-metal-free electrocatalysts for efficient energy conversion processes. Acc. Chem. Res. **50**, 915–923.
8. Li, M., Zhao, Z., Cheng, T., et al. (2016). Ultrafine jagged platinum nanowires enable ultrahigh mass activity for the oxygen reduction reaction. Science **354**, 1414–1419.
9. Chen, A., and Holt, H.P. (2010). Platinum-based nanostructured materials: synthesis, properties, and applications. Chem. Rev. **110**, 3767–3804.
10. Retuerto, M., Pascual, L., Calle-Vallejo, F., et al. (2019). Na-doped ruthenium perovskite electrocatalysts with improved oxygen evolution activity and durability in acidic media. Nat. Commun. **10**, 2041.
11. Escudero-Escribano, M., Malacrida, P., Hansen, M.H., et al. (2016). Tuning the activity of Pt alloy electrocatalysts by means of the lanthanide contraction. Science **352**, 73–76.
12. Tian, X., Luo, J., Nan, H., et al. (2016). Transition metal nitride coated with atomic layers of Pt as a low-cost, highly stable electrocatalyst for the oxygen reduction reaction. J. Am. Chem. Soc. **138**, 1575–1583.
13. Kang, P., Zhang, S., Meyer, T.J., et al. (2014). Rapid selective electrocatalytic reduction of carbon dioxide to formate by an iridium pincer catalyst immobilized on carbon nanotube electrodes. Angew. Chem. Int. Ed. **53**, 8709–8713.
14. Guo, X., Liu, P., Han, J., et al. (2015). 3D nanoporous nitrogen-doped graphene with encapsulated RuO_2 nanoparticles for Li-O_2 batteries. Adv. Mater. **27**, 6137–6143.
15. Khani, H., Grundish, N.S., Wipf, D.O., et al. (2019). Graphitic-shell encapsulation of metal electrocatalysts for oxygen evolution, oxygen reduction, and hydrogen evolution in alkaline solution. Adv. Energ. Mater. **10**, 1903215.
16. Jahan, M., Liu, Z., and Loh, K.P. (2013). A graphene oxide and copper-centered metal organic framework composite as a tri-functional catalyst for HER, OER, and ORR. Adv. Funct. Mater. **23**, 5363–5372.
17. Amiinu, I.S., Pu, Z., Liu, X., et al. (2017). Multifunctional Mo-N/C@MoS_2 electrocatalysts for HER, OER, ORR, and Zn-air batteries. Adv. Funct. Mater. **27**, 1702300.
18. Guo, Y., Yuan, P., Zhang, J., et al. (2018). Co_2P-CoN double active centers confined in N-doped carbon nanotube: heterostructural engineering for trifunctional catalysis toward HER, ORR, OER, and Zn-air batteries driven water splitting. Adv. Funct. Mater. **28**, 1805641.
19. Jia, Y., Zhang, L., Du, A., et al. (2016). Defect graphene as a trifunctional catalyst for electrochemical reactions. Adv. Mater. **28**, 9532–9538.
20. Rasaki, S.A., Zhang, B., Anbalgam, K., et al. (2018). Synthesis and application of nano-structured metal nitrides and carbides: a review. Prog. Solid State Chem. **50**, 1–15.
21. Ham, D.J., and Lee, J.S. (2009). Transition metal carbides and nitrides as electrode materials for low temperature fuel cells. Energies **2**, 873–899.
22. Liu, J. (2016). Porous Co_3Mo_3N nanorods as an effective electrocatalyst for Li-O_2 battery. Int. J. Electrochem. Sci. **11**, 498–505.
23. Zhang, K.Z.L., Dong, S., and Cui, G. (2013). In fabrication and application of metallic nitrides as cathode electrocatalysts for rechargeable Li-O_2 batteries. Adv. Optoelectron. Energy Environ.
24. Zha, Z., Cai, S., Wang, D., et al. (2013). Review on air cathode in Li-air batteries. J. Technol. Innov. Renew. Energ. **2**, 293–305.
25. Fu, X., Su, H., Yin, W., et al. (2017). Bimetallic molybdenum nitride Co_3Mo_3N: a new promising catalyst for CO_2 reforming of methane. Catal. Sci. Technol. **7**, 1671–1678.
26. Zeinalipouryazdi, C.D., and Catlow, C.R.A. (2017). A computational study of the heterogeneous synthesis of hydrazine on Co_3Mo_3N. Catal. Lett. **147**, 1820–1826.
27. Hada, K., Tanabe, J., Omi, S., et al. (2002). Characterization of cobalt molybdenum nitrides for thiophene HDS by XRD, TEM, and XPS. J. Catal. **207**, 10–22.
28. Podila, S., Zaman, S.F., Driss, H., et al. (2016). Hydrogen production by ammonia decomposition using high surface area Mo_2N and Co_3Mo_3N catalysts. Catal. Sci. Technol. **6**, 1496–1506.
29. Jacobsen, C.J., Dahl, S., Clausen, B.S., et al. (2001). Catalyst design by interpolation in the periodic table: bimetallic ammonia synthesis catalysts. J. Am. Chem. Soc. **123**, 8404–8405.
30. Amar, I.A.A., Lan, R., Petit, C.T., et al. (2015). Electrochemical synthesis of ammonia based on Co_3Mo_3N catalyst and $LiAlO_2$-(Li,Na,K)$_2CO_3$ composite electrolyte. Electrocatalysis **6**, 286–294.
31. Sun, T., Wu, Q., Che, R., et al. (2015). Alloyed Co-Mo nitride as high-performance electrocatalyst for oxygen reduction in acidic medium. ACS Catal. **5**, 1857–1862.
32. Hunter, S.M., Mckay, D., Smith, R.I., et al. (2010). Topotactic nitrogen transfer: structural transformation in cobalt molybdenum nitrides. Chem. Mater. **22**, 2898–2907.
33. Chen, P., Xu, K., Fang, Z., et al. (2015). Metallic Co_4N porous nanowire arrays activated by surface oxidation as electrocatalysts for the oxygen evolution reaction. Angew. Chem. Int. Ed. **54**, 14710–14714.
34. Pillai, S.B., Baraiya, B.A., Upadhyay;, D., et al. (2020). Catalytic activity and underlying atomic rearrangement in monolayer CoOOH towards HER and OER. Int. J. Hydrogen Energ. **45**, 23900–23907.
35. Zeinalipouryazdi, C.D., Hargreaves, J.S.J., and Catlow, C.R.A. (2016). DFT-D3 study of molecular N_2 and H_2 activation on Co_3Mo_3N surfaces. J. Phys. Chem. C **120**, 21390–21398.
36. Zeinalipouryazdi, C.D., Hargreaves, J.S.J., and Catlow, C.R.A. (2018). Low-T mechanisms of ammonia synthesis on Co_3Mo_3N. J. Phys. Chem. C **112**, 6078–6082.
37. Chen, Z., Song, Y., Cai, J., et al. (2018). Tailoring the d band centers enables Co_4N nanosheets to be highly active for hydrogen evolution catalysis. Angew. Chem. Int. Ed. **57**, 5076–5080.
38. Zhang, B., Zheng, X., Voznyy, O., et al. (2016). Homogeneously dispersed multimetal oxygen-evolving catalysts. Science **352**, 333–337.
39. Hammer, B., and Norskov, J.K. (1995). Electronic factors determining the reactivity of metal surfaces. Surf. Sci. **343**, 211–220.

40. Hammer, B., and Norskov, J.K. (2010). ChemInform abstract: theoretical surface science and catalysis-calculations and concepts. Cheminform *31*, 71–129.

41. Yu, P., Wang, L., Sun, F., et al. (2019). Co nanoislands rooted on Co-N-C nanosheets as efficient oxygen electrocatalyst for Zn-air batteries. Adv. Mater. *31*, 1901666.

42. Wei, Z.B.Z., Grange, P., and Delmon, B. (1998). XPS and XRD studies of fresh and sulfided Mo_2N. Appl. Surf. Sci. *135*, 107–114.

43. Baltrusaitis, J., Mendozasanchez, B., Fernandez, V., et al. (2015). Generalized molybdenum oxide surface chemical state XPS determination via informed amorphous sample model. Appl. Surf. Sci. *326*, 151–161.

44. Yuhong, W., Wei, L., Minghui, Z., et al. (2001). Characterization and catalytic properties of supported nickel molybdenum nitrides for hydrodenitrogenation. Appl. Catal. A Gen. *215*, 39–45.

45. Wang, M., Dong, C.-L., Huang, Y.-C., et al. (2020). Operando spectral and electrochemical investigation into the heterophase stimulated active species transformation in transition-metal sulfides for efficient electrocatalytic oxygen evolution. ACS Catal. *10*, 1855–1864.

46. Yu, X.-Y., Feng, Y., Guan, B., et al. (2016). Carbon coated porous nickel phosphides nanoplates for highly efficient oxygen evolution reaction. Energ. Environ. Sci. *9*, 1246–1250.

47. Yuan, Y., Adimi, S., Guo, X., et al. (2020). Surface oxide-rich activation layer (SOAL) on Ni_2Mo_3N for rapid and durable oxygen evolution reaction. Angew. Chem. Int. Ed. *59*, 18036–18041.

AUTHOR CONTRIBUTIONS

M.Y., F.J.D., and J.P.A. conceived and coordinated the research. Y.Y. synthesized and characterized the materials. S.A. performed electronic structure calculations. Y.Y., T.T., J.W., H.G., and J.C. carried out and analyzed the electrochemical measurements and co-wrote the paper with M.Y., F.J.D., and J.P.A. All authors discussed the results and commented on the manuscript.

DECLARATION OF INTERESTS

The authors declare no competing financial interests.

SUPPLEMENTAL INFORMATION

Supplemental information can be found online at https://doi.org/10.1016/j.xinn.2021.100096.

LEAD CONTACT WEBSITE

https://myang.nimte.ac.cn/.